

Chaotic and fractal properties of deterministic diffusion-reaction processes

P. Gaspard and R. Klages

*Center for Nonlinear Phenomena and Complex Systems
and Service de Chimie Physique,
Faculté des Sciences, Université Libre de Bruxelles,
Campus Plaine, Code Postal 231, B-1050 Brussels, Belgium
(January 20, 2022)*

We study the consequences of deterministic chaos for diffusion-controlled reaction. As an example, we analyze a diffusive-reactive deterministic multibaker and a parameter-dependent variation of it. We construct the diffusive and the reactive modes of the models as eigenstates of the Frobenius-Perron operator. The associated eigenvalues provide the dispersion relations of diffusion and reaction and, hence, they determine the reaction rate. For the simplest model we show explicitly that the reaction rate behaves as phenomenologically expected for one-dimensional diffusion-controlled reaction. Under parametric variation, we find that both the diffusion coefficient and the reaction rate have fractal-like dependences on the system parameter.

PACS numbers: 05.45.+b, 05.60.+w, 47.53.+n, 47.52.+j, 47.70.-n, 82.20.-w, 82.30.-b

Matter is most often the stage of reactions which evolve on a reactive time scale being intermediate between the long time scale of hydrodynamic transport phenomena and the short time scale of microscopic chaos. This chaos is generated by the collisions between the atoms and molecules of the fluid beyond a temporal horizon caused by the Lyapunov instability of motion. Under nonequilibrium conditions, long-time trajectories organize themselves in phase space to form fractal structures and weird invariant or conditionally invariant measures, the consequences of which have just started to be explored. In this perspective, we study here simple models of diffusion-reaction processes in order to confront the phenomenology with the new approach based on deterministic chaos.

I. INTRODUCTION

Irreversible phenomenological equations such as the Navier-Stokes or diffusion-reaction equations describe transport and reaction processes in fluid flows or chemical reactions occurring on macroscopic spatio-temporal scales. For instance, spatial inhomogeneities of size \mathcal{L} in the density are damped by diffusion over a time scale of the order of $T_{\text{diff}} \sim \mathcal{L}^2/D$, where D is the diffusion coefficient. In typical laboratory experiments, the size \mathcal{L} of the inhomogeneities is of the order of millimeters, centimeters, or larger so that the relaxation time T_{diff} is macroscopic.

Recent works have studied the relationship between these macroscopic processes and the much faster process of chaos in the microscopic motion of atoms or molecules in the fluid [1–7]. The defocusing character of the collisions between the particles of the fluid is at the origin of a very high dynamical instability in the microscopic motion. This instability, which is a major phenomenon at the center of the current interest, is characterized by a spectrum of positive Lyapunov exponents, as shown by many recent numerical and analytical studies [8–10]. The maximum Lyapunov exponent of a dilute gas of particles of diameter d is typically of the order of

$$\lambda_{\text{max}} \sim \frac{v}{\ell} \ln \frac{\ell}{d}, \quad (1)$$

where ℓ is the mean free path between the collisions, and v is the mean velocity of the particles [11,12]. Consequently, the time scale over which the dynamical instability develops in the motion of a particle due to the collisions with the surrounding particles is of the order of the inverse of the maximum Lyapunov exponent which takes the value $T_{\text{chaos}} \sim \lambda_{\text{max}}^{-1} \sim 10^{-10}$ sec for a gas at room temperature and pressure.

The microscopic time scale is in contrast with the macroscopic time scale of transport and reaction processes. This presence of two different time scales is an essential feature in the recent establishment of quantitative relationships between macroscopic transport and microscopic chaos in both the thermostatted-system and the escape-rate approaches [2–5,9,13–15]. Indeed, in both approaches transport coefficients are related to *differences* between two characteristic quantities of chaos: The thermostatted-system method works with the difference between the maximum and the absolute value of the minimum Lyapunov exponent [2,4,9], whereas the escape-rate approach employs the difference between the positive Lyapunov exponents and the Kolmogorov-Sinai entropy [3,5,13–15]. In this sense, the nonequilibrium property of transport is related to a slight disbalance between the dynamical instability, which is the cause,

and the induced temporal disorder, which is the effect. At equilibrium, the effect exactly compensates the cause. Away from equilibrium, temporal disorder is slightly reduced to the benefit of transport, which appears as an extra effect of the dynamical instability beside the temporal disorder. In this scheme, the fluid appears at the stage of a highly chaotic motion of its constituent particles, which animates different possible transport processes if the system is maintained out of equilibrium.

The hypothesis of microscopic chaos [12] or the chaotic hypothesis [16] replace the old stochastic hypotheses in nonequilibrium statistical mechanics. Previously, the stochastic hypotheses assumed that transport processes arise from stochastic effects, such as the Langevin white noise which has an infinite Kolmogorov-Sinai entropy per unit time. However, these processes have thus a much larger temporal disorder than allowed by Newton's deterministic equations of motion [17]. The new chaotic hypothesis has the enormous advantage of assuming a temporal disorder which is now compatible with the determinism of a microscopic Newtonian dynamics. In this regard, the chaotic hypothesis overwhelms the previous stochastic hypotheses, which nevertheless remains of great usefulness in their domain of validity.

The purpose of the present paper is to describe several consequences of the hypothesis of microscopic chaos in diffusion-reaction systems. This class of physico-chemical processes has not yet been explored in the perspective of understanding their kinetics on the sole assumption of microscopic chaos, without involving stochastic Langevin or birth-and-death processes. The diffusion-reaction systems are particularly important in various fields of chemical physics, such as chemical kinetics, homogeneous and heterogeneous catalyses, pattern formation in nonequilibrium reactions and in morphogenesis, recombination processes in solid or liquid phases, as well as high-energy reaction processes in astrophysical systems [18].

We shall focus here on the simplest diffusion-reaction process with a linear chemical reaction law,



which already provides a nontrivial dynamics. As a vehicle of our study we shall use multibaker models, which are deterministic versions of discrete Markov processes. The deterministic dynamics of a multibaker has therefore the same finite and positive Kolmogorov-Sinai entropy per unit time as the corresponding discrete Markov process. The models we propose are spatially extended generalizations of a baker-type model of isomerization previously studied by Elskens and Kapral [19].

This paper is organized in the following way: In Section II, we construct multibaker models of diffusion-reaction by starting from a diffusive-reactive Lorentz gas. In Section III, we focus on the diffusive properties of the multibakers. By employing quasiperiodic boundary conditions we show that for the simplest model the diffusive properties are the same as those of the previously discussed dyadic multibaker of diffusion. We then demonstrate that under parametric variation of this model the diffusion coefficient exhibits a self-similar structure reminiscent of fractal curves. In Section IV, we describe the reactive properties. With quasiperiodic boundary conditions, we first study the simplest model and derive the dispersion relation of the chemodynamic modes. We explicitly construct the phase-space distribution of these modes and define the reaction rate by comparison with phenomenology. We then show that the reaction rate behaves in a highly irregular manner if we consider the parameter-dependent model. Conclusions are drawn in Section V.

II. DETERMINISTIC MODELS OF DIFFUSION-REACTION PROCESSES

A. Definition of the models

In order to motivate the introduction of the multibaker models, we first consider a reactive Lorentz gas in which a point particle undergoes elastic collisions on hard disks which are fixed in the plane. The disks may form a random or a regular configuration (Fig. 1). A fraction of the disks are supposed to be catalysts where the point particle changes its state, or color, from A to B or vice versa at the instant of the collision. The mass of the particle is assumed to be the same in both states A and B . The phase space coordinates of each particle are given by its position, its velocity, and its color (x, y, v_x, v_y, c) with $c \in \{A, B\}$. Since energy is conserved at the elastic collisions, the magnitude of the velocity is a constant of motion, $v = \sqrt{v_x^2 + v_y^2}$, so that the coordinates reduce to $(x, y, \varphi, c) = (\mathbf{X}, c)$, where $\varphi = \arctan(v_y/v_x)$ is the angle between the velocity and the x -axis.

The motion induces a time evolution of the phase-space probability densities, or concentrations, for each color,

$$\mathbf{f}(\mathbf{X}) = \begin{pmatrix} f(\mathbf{X}, A) \\ f(\mathbf{X}, B) \end{pmatrix}. \quad (3)$$

The mean phase-space density, defined by the average of the concentrations, does not distinguish between the colors. Thus, we may expect that

$$\tilde{f}(\mathbf{X}) = \frac{1}{2}[f(\mathbf{X}, A) + f(\mathbf{X}, B)] \quad (4)$$

evolves in time exactly as in the non-reactive Lorentz gas, as studied elsewhere [20–22]. The dynamics of reaction should appear in the difference between the concentrations

$$g(\mathbf{X}) = f(\mathbf{X}, A) - f(\mathbf{X}, B) \quad (5)$$

which is expected to follow a macroscopic relaxation toward zero if there is equipartition of particles between both colors.

It has been explained elsewhere that the flow dynamics of the Lorentz gas can be reduced to a Birkhoff mapping from collision to collision [22]. Each collision can be represented by two variables: the angle θ giving the position of impact on the perimeter of the disk as $(x = \cos \theta, y = \sin \theta)$ and the angle ϕ between the velocity after the collision and the normal at impact. The sine of the velocity angle $\varpi = \sin \phi$ together with the position angle θ are the so-called Birkhoff coordinates, in which the mapping is area-preserving. All the collision events with the disk of label l are thus represented by the rectangle

$$\mathcal{R}_l = \{(\theta, \varpi, l) : 0 \leq \theta < 2\pi, -1 \leq \varpi \leq +1\}. \quad (6)$$

The dynamics of collisions can therefore be written as the Birkhoff mapping

$$(\theta_{n+1}, \varpi_{n+1}, l_{n+1}, c_{n+1}) = \Phi(\theta_n, \varpi_n, l_n, c_n), \quad (7)$$

which is known to be area-preserving, time-reversal symmetric, and of hyperbolic character.

A caricature of this mapping is provided by a multibaker model (Fig. 2) in which we suppose that the rectangular domains Eq. (6) representing the disks are replaced by squares

$$\mathcal{S}_l = \{(x, y, l) : 0 \leq x \leq 1, 0 \leq y \leq 1\}, \quad (8)$$

where $l \in \mathbb{Z}$ is the label of the square. Each square of the multibaker model corresponds to a disk of the Lorentz gas. Now, the collision dynamics is simplified by replacing the complicated Birkhoff map Eq. (7) by a baker-type map with horizontal stretching by a factor of two, followed by cutting the elongated square into two. The collisions from disk to disk are replaced by jumps of the particle from square to square according to the transition rule $l \rightarrow l - 1$ if $x \leq 1/2$ and $l \rightarrow l + 1$ if $x > 1/2$ between next-neighboring squares. The squares are arranged such that they form a one-dimensional chain. One out of L squares is assumed to be a catalyst where the color changes from $c = A$ (resp. B) to its complement $\bar{c} = B$ (resp. A). The map of the model is thus

$$\Phi(x, y, l, c) = \begin{cases} \left(2x, \frac{y}{2}, l - 1, c'\right), & 0 \leq x \leq \frac{1}{2}, \\ \left(2x - 1, \frac{y+1}{2}, l + 1, c'\right), & \frac{1}{2} < x \leq 1, \end{cases} \quad (9)$$

where $c' = \bar{c}$ if $l = 0, \pm L, \pm 2L, \dots$ and $c' = c$ otherwise. This map is area-preserving, time-reversal symmetric, and chaotic with a positive Lyapunov exponent $\lambda_+ = \ln 2$ and a negative one $\lambda_- = -\ln 2$, such as the multibaker map [23–26].

In our model, the reaction is controlled by the diffusion if the reactive sites are diluted in the system. This important case of chemical reactions has been much studied in the literature since Smoluchowski seminal work [27]. It is known that the macroscopic reaction rate is determined by the time taken by particles to diffuse toward the reactive site. A crossover occurs at dimension two which is the Hausdorff dimension of a Brownian path. Accordingly, the flux of reactants toward a catalyst is sensitive to the presence of the next-neighboring catalysts in less than two dimensions, but not in systems of dimensions higher than two. In particular, in a one-dimensional system the reaction rate should behave as

$$\kappa \sim \frac{D}{L^2}, \quad (10)$$

where D is the diffusion coefficient and L is the distance between the reactive sites or catalysts.

A main goal of our work is to investigate the dynamical properties of our diffusion-reaction model in order to know whether this expected macroscopic behavior is confirmed from the microscopic dynamics or not. We shall also

consider a parametric variation of this model with a more complicated dynamics. This is due to an extra dependency on a shift parameter which is introduced when the half squares are glued back into the chain. When this continuous parameter varies it induces topological changes in the trajectory dynamics which are reminiscent of the topological changes induced by varying the disk radius in the Lorentz gas [20–22]. The parametric extension of the multibaker model shows that the diffusion coefficient as well as the reaction rate may vary in a highly irregular fashion as a function of a parameter. This is an important consequence of deterministic chaos which already appears on the level of one-dimensional maps, as will be discussed in the following section.

B. The Frobenius-Perron operator and quasiperiodic boundary conditions

Since Boltzmann's work, it is well known that transport and reaction-rate processes should be conceived in a statistical sense because the individual trajectories are affected by the famous Poincaré recurrences. We therefore consider the time evolution of statistical ensembles of trajectories as represented by the probability densities Eq. (3). They evolve in time according to the Frobenius-Perron equation

$$f_{t+1}(x, y, l, c) = f_t \left[\Phi^{-1}(x, y, l, c) \right] \equiv (\hat{P} f_t)(x, y, l, c) \quad (t \in \mathbb{Z}) . \quad (11)$$

We choose quasiperiodic boundary conditions by assuming that the solution of the Frobenius-Perron equation is quasiperiodic on the chain with a wavenumber k . Moreover, we suppose that the solution decays exponentially with a decaying factor $\chi = \exp s$ where $|\chi| \leq 1$ or $\text{Re } s \leq 0$,

$$f_t(x, y, l, c) \sim \chi^t \exp(ikl) . \quad (12)$$

The decay rate s is calculated by solving the eigenvalue problem of the Frobenius-Perron operator. We note that the Frobenius-Perron operator is in general non-unitary so that root vectors associated with possible Jordan-block structures may exist beyond the eigenvectors. We shall focus here on the eigenvectors because they control the slowest decay on the longest time scales [24,25].

For quasiperiodic solutions, the Frobenius-Perron operator reduces to the following Frobenius-Perron operator \hat{Q}_k which depends on the wavenumber k and acts on functions which are defined only in L successive squares of the chain,

$$\hat{Q}_k \equiv \begin{cases} f_{t+1}(x, y, 0, c) = \theta\left(\frac{1}{2} - y\right) f_t\left(\frac{x}{2}, 2y, 1, c\right) + e^{-ikL} \theta\left(y - \frac{1}{2}\right) f_t\left(\frac{x+1}{2}, 2y-1, L-1, c\right) , \\ f_{t+1}(x, y, 1, c) = \theta\left(\frac{1}{2} - y\right) f_t\left(\frac{x}{2}, 2y, 2, c\right) + \theta\left(y - \frac{1}{2}\right) f_t\left(\frac{x+1}{2}, 2y-1, 0, \bar{c}\right) , \\ f_{t+1}(x, y, 2, c) = \theta\left(\frac{1}{2} - y\right) f_t\left(\frac{x}{2}, 2y, 3, c\right) + \theta\left(y - \frac{1}{2}\right) f_t\left(\frac{x+1}{2}, 2y-1, 1, c\right) , \\ \vdots \\ f_{t+1}(x, y, L-2, c) = \theta\left(\frac{1}{2} - y\right) f_t\left(\frac{x}{2}, 2y, L-1, c\right) + \theta\left(y - \frac{1}{2}\right) f_t\left(\frac{x+1}{2}, 2y-1, L-3, c\right) , \\ f_{t+1}(x, y, L-1, c) = e^{ikL} \theta\left(\frac{1}{2} - y\right) f_t\left(\frac{x}{2}, 2y, 0, \bar{c}\right) + \theta\left(y - \frac{1}{2}\right) f_t\left(\frac{x+1}{2}, 2y-1, L-2, c\right) . \end{cases} \quad (13)$$

We notice that there is a reaction, i.e., a change of color, for particles passing the cell $l = 0$ so that a concentration with $l = 0$ and \bar{c} appears in the second and in the last line. We also notice that there is a factor $\exp(-ikL)$ in the first line for the particle coming from the previous segment of length L in the infinite chain, where the concentration functions are multiplied by the factor $\exp(-ikL)$. On the other hand, there is a factor $\exp(ikL)$ in the last line for the particle coming from the next segment where the concentration functions are multiplied by $\exp(ikL)$. Otherwise, this Frobenius-Perron operator is the same as in the infinite dyadic multibaker model studied in Refs. [23–25].

As we discussed in the previous section, the presence of two chemical components $c = A$ or B implies that the Frobenius-Perron operator \hat{Q}_k acts on $2L$ functions which can be linearly combined to separate the functional space in two subspaces on which two decoupled Frobenius-Perron operators would act. The first subspace is defined by Eq. (4) where the Frobenius-Perron operator reduces to the diffusive Frobenius-Perron operator of the multibaker map. The second subspace is defined by Eq. (5) which gives a different evolution operator of reactive type. Diffusive properties are studied in the next Section III, while reactive properties will be discussed in Section IV.

III. DIFFUSION DYNAMICS

A. Diffusive modes of the dyadic multibaker

In this subsection, we consider the diffusive dynamics of the dyadic multibaker model Eq. (9) with quasiperiodic boundary conditions. The subspace of diffusion is defined by the mean density of Eq. (4). For hydrodynamic modes of wavenumber k we thus write

$$\tilde{f}_t(x, y, l) = \frac{1}{2} [f_t(x, y, l, A) + f_t(x, y, l, B)] \equiv \exp \left[i \left(k + 2\pi \frac{\nu}{L} \right) l \right] \eta_t(x, y) , \quad (14)$$

and the new function obeys the simpler evolution equation

$$\eta_{t+1}(x, y) = (\hat{Q}_k^{(D)} \eta_t)(x, y) \equiv e^{+i(k+2\pi\nu/L)} \theta\left(\frac{1}{2} - y\right) \eta_t\left(\frac{x}{2}, 2y\right) + e^{-i(k+2\pi\nu/L)} \theta\left(y - \frac{1}{2}\right) \eta_t\left(\frac{x+1}{2}, 2y-1\right) , \quad (15)$$

which is the Frobenius-Perron equation for the dyadic multibaker map based on quasiperiodic boundary conditions [24]. The respective Frobenius-Perron operator has been analyzed in detail elsewhere [24,25]. Its decay rates are

$$s_{m\nu}(k) = \ln \chi_{m\nu}(k) = -m \ln 2 + \ln \cos \left(k + \frac{2\pi\nu}{L} \right) \quad (16)$$

with $m = 0, 1, 2, 3, \dots$, $\nu = 0, 1, 2, \dots, L-1$, and with a degeneracy of $(m+1)$. The eigenvectors

$$(\hat{Q}_k^{(D)} \psi_{m\nu})(x, y; k) = e^{s_{m\nu}(k)} \psi_{m\nu}(x, y; k) , \quad (17)$$

and some root vectors have been constructed in Refs. [24,25] in terms of the cumulative functions

$$F_{0\nu}(x, y; k) = \int_0^x dx' \int_0^y dy' \psi_{0\nu}(x', y'; k) . \quad (18)$$

For small enough wavenumbers k , these cumulative functions are continuous functions which are products of a monomial in x with a nondifferentiable de Rham function in y . Accordingly, the eigenvectors $\psi_{0\nu}$ are complex singular measures for small enough k .

We observe that the decay rate with $m = 0$ and $\nu = 0$ vanishes quadratically as $k \rightarrow 0$ in agreement with the expected diffusive behavior,

$$s_{00}(k) = \ln \cos k = -\frac{k^2}{2} - \frac{k^4}{12} \dots , \quad (19)$$

which shows that the diffusion coefficient is $D = 1/2$.

The nonequilibrium steady states corresponding to a uniform density gradient g for the mean density of Eq. (4) have also been constructed [26]. It has been shown that the nonequilibrium steady state of the infinite system corresponds to a singular invariant measure represented by a continuous but nondifferentiable cumulative function

$$F_{\text{st. st.}}(x, y, l) = \int_0^x dx' \int_0^y dy' \tilde{f}_{\text{st. st.}}(x', y', l) = g l x y + g x T(y) , \quad (20)$$

where $T(y)$ is the Takagi function obtained as a solution of the iteration [28]

$$T(y) = \begin{cases} \frac{1}{2} T(2y) + y , & 0 \leq y \leq \frac{1}{2} , \\ \frac{1}{2} T(2y-1) - y + 1 , & \frac{1}{2} < y \leq 1 . \end{cases} \quad (21)$$

The Takagi function is nondifferentiable because its formal derivative is infinite almost everywhere. It is given by a Lebowitz-McLennan type of formula [29]

$$\frac{dT}{dy} = \sum_{t=0}^{\infty} j[M^t(y)] , \quad (22)$$

where $M(y) = (2y)$ (modulo 1), and $j(y) = \pm 1$ if $y < 1/2$ or $y > 1/2$, respectively, is the *jump-velocity*. The singular character of the diffusive steady state turns out to be a general feature in finite-dimensional deterministic chaos of large spatial extension, as shown elsewhere [22,26].

Moreover, this singular character of the steady state measure plays a fundamental role in the explanation of the entropy production of irreversible thermodynamics. In particular, the expected entropy production can be derived from the Takagi function in the case of the multibaker map [30]. The presence of this singularity solves the famous paradox of the constancy of the Gibbs entropy, which can be set up when we do not recognize that the out-of-equilibrium invariant measure is very different from the equilibrium one on fine scales in phase space. The out-of-equilibrium invariant measure becomes singular if the nonequilibrium constraints are imposed at distances larger than several mean free paths. This is probably a paradoxical aspect of the local equilibrium hypothesis that a nonequilibrium system appears in local equilibrium on the largest scales of phase space although intrinsic correlations exist on finer scales which are due to the chaotic dynamics. The singular character of the invariant measure explains that there is an entropy production in large nonequilibrium systems where the chaotic dynamics removes the signature of determinism down to extremely fine scales in phase space.

B. Diffusion coefficients in parameter-dependent models

In this subsection, we describe an important consequence of deterministic chaos which shows up when a system parameter is varied. Under such circumstances, the diffusion coefficient of maps like a parameter-dependent multibaker exhibits a fractal structure by changing the parameter. In the same way as outlined in this subsection, we will show later that the same behavior appears in the reactive transport properties of our parameter-dependent multibaker. We thus emphasize the striking analogies between the diffusive and the reactive properties in regard to their parametric sensitivity.

For this purpose, we summarize the main methods and results concerning the parametric variation of the diffusive dynamics in multibakers and in simple one-dimensional maps. To study parameter-dependent transport in multibaker models like Eq. (9) such one-dimensional maps are crucial, because they govern the dynamics of multibakers projected onto the x -axis. We therefore start with a brief review on parameter-dependent diffusion in one-dimensional maps. We then show how all the methods and results obtained for one-dimensional maps carry over to a two-dimensional parameter-dependent multibaker which we introduce and discuss to the end of this subsection.

1. Fractal forms in a Green-Kubo formula

Chains of one-dimensional chaotic maps are the simplest dynamical systems in which deterministic diffusion can be studied [31]. One may think of them as deterministic generalizations of simple random walks on the real line, where the full microscopic history of the particles is taken into account. In general, the microscopic dynamics is affected by changes of some control parameters. Hence, in contrast to the discussion of the previous subsection where no parameter has been varied, we will be interested here in the resulting parameter dependence of the diffusion coefficient [6,32–35]. As mentioned before, the parameters to be considered may be physically related to, for instance, varying the density or the shape of scatterers. An example of such systems is the chain of piecewise linear maps depicted in Fig. 3. This map is of the general form $x_{t+1} = M_a(x_t)$, and it is periodic by satisfying the condition $M_a(x+1) = M_a(x) + 1$. The slope a serves as the control parameter and is trivially related to the Lyapunov exponent of the map via $\lambda = \ln a$. The parameter-dependent diffusion coefficient can be obtained by the Green-Kubo formula [1,23,32,35]

$$D(a) \equiv \left\langle j_a(x) \sum_{t=0}^{\infty} j_a[M_a^t(x)] \right\rangle - \frac{1}{2} \langle j_a^2(x) \rangle \quad , \quad (23)$$

where the average $\langle \cdot \rangle \equiv \int_0^1 dx \, \varrho_a(x) (\cdot)$ has to be taken over the invariant probability density $\varrho_a(x)$ on the unit interval. $j_a(x)$ gives the integer number of boxes a particle has traversed after one iteration starting at position x and is thus the parameter-dependent extension of the jump-velocity introduced in Eq. (22) above. Thus, the complete microscopic dynamics is divided into two parts in Eq. (23): the *intra-cell dynamics*, that is, the dynamics within a single box, which is represented by the invariant probability density, and the *inter-cell dynamics* given by the sum of the jump-velocities, which contains the history of the particles travelling between the single boxes of the chain.

For computing the diffusion coefficient both parts can be treated separately. The invariant probability density is obtained by solving the Frobenius-Perron equation for the map restricted to the unit interval, $\tilde{M}_a(x) \equiv M_a(x) \pmod{1}$,

$$\varrho_{a,t+1}(x) = \int dz \varrho_{a,t}(z) \delta[x - \tilde{M}_a(z)] \quad . \quad (24)$$

To do this, Eq. (24) can be written as a matrix equation, where the Frobenius-Perron operator has been transformed into a transition matrix [6,23,32,36]. For maps of the type considered here, exact transition matrices can be constructed whenever a so-called Markov partition exists. This is the case for a dense set of parameter values a on the real line. The invariant probability density can then be calculated either by solving the eigenvalue problem of the transition matrix, which in simple cases can be performed analytically, or by solving the Frobenius-Perron equation by iterating the transition matrices numerically [37].

In Fig. 4 (a) and (b), typical invariant probability densities are plotted at two values of the slope. They are step functions on the unit interval, where the regions of the functions being piecewise constant correspond to the single cells of the respective Markov partitions. For piecewise linear maps, the invariant probability densities should always be step functions, although for arbitrary parameter value they may consist of infinitely many steps [32,38,39]. The sum of jump-velocities, as the second ingredient of the Green-Kubo formula Eq. (23), gives the integer displacement of a particle after t iterations starting at initial position x . Since the system is chaotic, this function is highly irregular in x . To deal with this quantity, it is more convenient to define functions $T_a(x)$ via

$$\frac{dT_a}{dx} \equiv \sum_{t=0}^{\infty} j_a[M_a^t(x)] \quad , \quad (25)$$

which is a parametric extension of Eq. (22). The functions $T_a(x)$ now give the integral of the displacement of particles which start in a certain subinterval, and they behave much more regular in x than the sums of jumps. Employing $T_a(x) = \lim_{t \rightarrow \infty} T_{a,t}(x)$, it can be shown that these functions are obtained in terms of the recursion relation

$$T_{a,t}(x) = t_a(x) + \frac{1}{a} T_{a,t-1}[\tilde{M}_a(x)] \quad , \quad (26)$$

with $t_a(x)$ being determined by $dt_a/dx \equiv j_a(x)$ and by requiring that $T_a(0) = T_a(1) = 0$. $T_a(x)$ can be computed by iterating Eq. (26) numerically. For two special values of the slope the results have been plotted in Fig. 4 (c) and (d). The functions $T_a(x)$ are self-similar on the unit interval and scale with the slope a . For $a = 2$, Eq. (26) appears as a special case of Eq. (21). Therefore, functions like $T_a(x)$ may be denoted as *generalized Takagi functions*.

The numerically exact result for the parameter-dependent diffusion coefficient is shown in Fig. 5 for $2 \leq a \leq 8$. Naively, one may have expected that $D(a)$ increases monotonically by increasing the slope. But this is only the case on a sufficiently coarse grained scale, where $D(a)$ can in fact be qualitatively matched to the results of two simple random walk models [33]. On a fine scale, however, $D(a)$ shows a complicated structure with different regions exhibiting different kinds of self-similarity. A numerical estimation shows that the curve has a fractal dimension which is very close to, but greater than one.

This highly irregular behavior of $D(a)$ is caused by correlations of increasingly higher order in the microscopic dynamics of the map. For instance, in the initial region $2 \leq a \leq 3$, which has been magnified in Fig. 5, the fine structure can be physically explained by relating local extrema on the curve to characteristics of the microscopic scattering process in one box as it changes with the parameter a [6,32]: if stronger *backscattering* sets in by making a larger, the curve exhibits a local maximum, if stronger *forward scattering* occurs, it goes through a local minimum.

More generally, the fractal character of $D(a)$ can be understood by analyzing the Green-Kubo Eq. (23) [32,35]. Two basic components in the formula are responsible for the fractal character of the curve: On the one hand, the diffusion coefficient is given in terms of sums of jumps, which, according to Eq. (25), are related to fractal generalized Takagi functions as shown in Fig. 4 (a) and (b). This goes together with the jump velocity $j_a(x)$ having a discontinuity which varies with the parameter a and which reveals in a sense the fractal character of the generalized Takagi functions. On the other hand, a second source of irregularity are the stepwise discontinuities in the density of the invariant measure $\varrho_a(x)$ as shown in Fig. 4 (c) and (d). The irregular behavior of the diffusion coefficient results from a combination of these effects, which are connected in the Green-Kubo formula via integrating the respective generalized Takagi functions over the respective invariant density. Thus, actually this behavior finds its origin in the non-robustness of the topology of the trajectories under parametric perturbations.

2. A time-reversible area-preserving multibaker with fractal diffusion coefficients

The same phenomenon of a fractal diffusion coefficient appears in a parameter-dependent generalization of the diffusive-reactive multibaker model introduced above [34]. This two-dimensional area-preserving map is sketched in

Fig. 6. Here, the two rectangles of the left and of the right half of the square are “sliding” along the upper and the lower horizontal channel of the periodically continued map governed by a parameter h , as shown in the figure. It should be noted that for $h = 0.5$ and shifting the coordinate system by $\Delta x = 0.5$ the model reduces to the simple dyadic multibaker of Eq. (9). The dynamics of the probability density $\tilde{f}_t(x, y, l)$ of the full multibaker $\Phi_h(x, y, l)$ is determined by the Frobenius-Perron equation $\tilde{f}_{t+1}(x, y, l) = \tilde{f}_t[\Phi_h^{-1}(x, y, l)]$, where $\Phi_h^{-1}(x, y, l)$ is the inverse map. A projection of this two-dimensional Frobenius-Perron equation onto the unstable x -direction by integrating over the stable y -direction via $\varrho_t(x, l) \equiv \int dy \tilde{f}_t(x, y, l)$ [1,23] shows that the dynamics of the probability density $\varrho_t(x, l)$ is determined by the Frobenius-Perron equation of the simple one-dimensional map included in Fig. 6, which is a kind of Bernoulli map shifted symmetrically by a height h . This one-dimensional map governs the dynamics of the multibaker map projected on the x -axis. By extending the system periodically, we recover a chain of one-dimensional maps of the type of the one shown in Fig. 3. Concerning time-reversibility, we follow the definition that there must exist an involution \mathbf{G} in phase space, $\mathbf{G} \circ \mathbf{G} = 1$, which reverses the direction of time via $\mathbf{G} \circ \Phi \circ \mathbf{G} = \Phi^{-1}$ [40]. For the special case of h taking multiples of $1/2$ involutions \mathbf{G} can be found which are related to a simple mirroring in phase space [41]. For general h , it can be shown that the system has strong time-reversible properties, although the existence of an involution \mathbf{G} remains an open question [34,40].

To compute the parameter-dependent diffusion coefficient of this multibaker we use that the projected dynamics is governed by a one-dimensional map, and thus we apply the same methods as outlined above. The result is shown in Fig. 7. The diffusion coefficient is again a non-trivial function of the parameter h and shares many characteristics of the curve presented in Fig. 5, for example, a certain random walk-like behavior on a coarse grained scale [33]. But it also exhibits some new features, especially that the diffusion coefficient is constant in intervals $0.5 + m \leq h \leq 1 + m$, $m \in \mathbb{N}_0$. This is due to the fact that the transition matrices corresponding to respective Markov partitions, and thus the respective symbolic dynamics of the map, do not change in this parameter interval. It is worth mentioning that in contrast to the specific model of Fig. 3 the invariant probability density of the projected one-dimensional map here is always uniform for all parameter values of h . Therefore, the only contributions to the fractality of $D(h)$ come from the inter-cell dynamics as described by the Takagi functions $T_a(x)$.

Along the same lines as above, we can also consider parametric variations of a bias in one-dimensional maps and in multibaker models [34,38,42,43]. In these systems, the deterministic dynamics appears in form of currents which are fractal functions of the bias, in certain parameter regions the mean current can run opposite to the bias, and the diffusion coefficient can be zero with non-zero current [34,38,42]. In this regard, it is interesting to point out that drift currents which are irregularly fluctuating by varying the bias have also been observed numerically in other deterministic models [44]. Moreover, we notice that certain biased maps can be related to so-called ratchets [42,45].

IV. REACTIVE DYNAMICS

A. Reactive modes of the dyadic multibaker

In this section, we turn to the study of the chemiodynamic or reactive modes of our simple dyadic model Eq. (9) of diffusion-controlled reaction. Contrary to the total number of particles, $N_A + N_B$, which is a constant of motion, the numbers of particles of each chemical species are not conserved. Accordingly, we should not expect that the reactive modes have a vanishing decay rate as $k \rightarrow 0$. This is in contrast to the diffusive modes which are related to the conserved total number of particles and for which the decay rate (19) vanishes at $k = 0$.

Here, we consider the subspace defined by the difference between the particle concentrations in the multibaker,

$$g(x, y, l) \equiv f(x, y, l, A) - f(x, y, l, B). \quad (27)$$

Thus, we employ the fact that the dynamics of the concentration difference can be decoupled from the mean density for this model, as has been mentioned before, compare to Eq. (5).

With quasiperiodic boundary conditions, the difference of chemical concentration evolves in time according to the reactive evolution operator

$$\hat{R}_k \equiv \begin{cases} g_{t+1}(x, y, 0) = \theta\left(\frac{1}{2} - y\right) g_t\left(\frac{x}{2}, 2y, 1\right) + e^{-ikL} \theta\left(y - \frac{1}{2}\right) g_t\left(\frac{x+1}{2}, 2y-1, L-1\right), \\ g_{t+1}(x, y, 1) = \theta\left(\frac{1}{2} - y\right) g_t\left(\frac{x}{2}, 2y, 2\right) - \theta\left(y - \frac{1}{2}\right) g_t\left(\frac{x+1}{2}, 2y-1, 0\right), \\ g_{t+1}(x, y, 2) = \theta\left(\frac{1}{2} - y\right) g_t\left(\frac{x}{2}, 2y, 3\right) + \theta\left(y - \frac{1}{2}\right) g_t\left(\frac{x+1}{2}, 2y-1, 1\right), \\ \vdots \\ g_{t+1}(x, y, L-2) = \theta\left(\frac{1}{2} - y\right) g_t\left(\frac{x}{2}, 2y, L-1\right) + \theta\left(y - \frac{1}{2}\right) g_t\left(\frac{x+1}{2}, 2y-1, L-3\right), \\ g_{t+1}(x, y, L-1) = -e^{ikL} \theta\left(\frac{1}{2} - y\right) g_t\left(\frac{x}{2}, 2y, 0\right) + \theta\left(y - \frac{1}{2}\right) g_t\left(\frac{x+1}{2}, 2y-1, L-2\right). \end{cases} \quad (28)$$

Our goal is here to obtain the eigenvalues and eigenstates of this reactive evolution operator

$$\hat{R}_k \{\Psi(x, y, l)\}_{l=0}^{L-1} = e^{s(k)} \{\Psi(x, y, l)\}_{l=0}^{L-1}, \quad (29)$$

with $\chi(k) = \exp[s(k)]$. We define the cumulative functions

$$G_t(x, y, l) = \int_0^x dx' \int_0^y dy' g_t(x', y', l), \quad (30)$$

which obey a set of equations which can be derived from Eq. (28). We suppose that the leading eigenstates are uniform along the unstable direction x , which is justified by the fact that the hyperbolic dynamics smoothens out any heterogeneities along the unstable direction,

$$\Psi(x, y, l) = \mathcal{D}(y, l), \quad (31)$$

where $\mathcal{D}(y, l)$ is a Schwartz distribution. We note that the further eigenstates and root states do depend on x and require a more detailed analysis. The cumulative functions of the leading eigenstates are thus

$$G_{\text{eigenstate}}(x, y, l) \equiv x C(y, l) \quad \text{with} \quad C(y, l) = \int_0^y dy' \mathcal{D}(y', l). \quad (32)$$

Replacing $g_t(x, y, l)$ by $\mathcal{D}(y, l)$ and $g_{t+1}(x, y, l)$ by $\chi \mathcal{D}(y, l)$ in Eq. (28) and integrating over the interval $[0, y]$, we obtain the following iterative equations for the new functions $C(y, l)$

$$\begin{cases} C(y, 0) = \begin{cases} \frac{1}{2\chi} C(2y, 1), & y < 1/2, \\ \frac{1}{2\chi} [C(1, 1) + \exp(-ikL)C(2y-1, L-1)], & y > 1/2, \end{cases} \\ C(y, 1) = \begin{cases} \frac{1}{2\chi} C(2y, 2), & y < 1/2, \\ \frac{1}{2\chi} [C(1, 2) - C(2y-1, 0)], & y > 1/2, \end{cases} \\ C(y, 2) = \begin{cases} \frac{1}{2\chi} C(2y, 3), & y < 1/2, \\ \frac{1}{2\chi} [C(1, 3) + C(2y-1, 1)], & y > 1/2, \end{cases} \\ \vdots \\ C(y, L-2) = \begin{cases} \frac{1}{2\chi} C(2y, L-1), & y < 1/2, \\ \frac{1}{2\chi} [C(1, L-1) + C(2y-1, L-3)], & y > 1/2, \end{cases} \\ C(y, L-1) = \begin{cases} -\frac{\exp(ikL)}{2\chi} C(2y, 0), & y < 1/2, \\ \frac{1}{2\chi} [-\exp(ikL)C(1, 0) + C(2y-1, L-2)], & y > 1/2. \end{cases} \end{cases} \quad (33)$$

The eigenvalue can be obtained by setting $y = 1$ in Eq. (33), which leads to the eigenvalue equation

$$\begin{pmatrix} -2\chi & 1 & 0 & 0 & \cdots & 0 & 0 & \exp(-ikL) \\ -1 & -2\chi & 1 & 0 & \cdots & 0 & 0 & 0 \\ 0 & 1 & -2\chi & 1 & \cdots & 0 & 0 & 0 \\ 0 & 0 & 1 & -2\chi & \cdots & 0 & 0 & 0 \\ \vdots & \vdots & \vdots & \vdots & \ddots & \vdots & \vdots & \vdots \\ 0 & 0 & 0 & 0 & \cdots & 1 & -2\chi & 1 \\ -\exp(ikL) & 0 & 0 & 0 & \cdots & 0 & 1 & -2\chi \end{pmatrix} \begin{pmatrix} C(1, 0) \\ C(1, 1) \\ C(1, 2) \\ C(1, 3) \\ \vdots \\ C(1, L-2) \\ C(1, L-1) \end{pmatrix} = 0. \quad (34)$$

The characteristic determinant has been calculated for several values of the distance L between the reactive sites,

$$L = 3 : \quad 4\chi^3 + \chi + \cos(3k) = 0 , \quad (35)$$

$$L = 4 : \quad 8\chi^4 - 2 + 2\cos(4k) = 0 , \quad (36)$$

$$L = 5 : \quad 16\chi^5 - 4\chi^3 - 3\chi + \cos(5k) = 0 , \quad (37)$$

$$L = 6 : \quad 32\chi^6 - 16\chi^4 - 6\chi^2 + 1 + \cos(6k) = 0 , \quad (38)$$

\vdots

The corresponding dispersion relations of the reactive modes are depicted in Fig. 8 together with those of the diffusive modes. Fig. 8 shows that the slowest decay rate which gives the reaction rate appears at $k = 0$ for L odd and at $k = \pm\pi/L$ for L even. The cumulative functions $\{C(y, l)\}_{l=0}^3$ of the eigenstate corresponding to the reaction rate at $k = 0$ are depicted in Fig. 9 for the model with $L = 3$ by solving Eq. (33) iteratively. Near its maximum values, the dispersion relation behaves quadratically like

$$L \text{ odd} : \quad s^{(r)}(k, L) = -\tilde{\kappa}(L) - D^{(r)}(L) k^2 + \mathcal{O}(k^4) \quad \text{at } k = 0 , \quad (39)$$

$$L \text{ even} : \quad s^{(r)}(k, L) = -\tilde{\kappa}(L) - D^{(r)}(L) (k \mp \pi/L)^2 + \mathcal{O}[(k \mp \pi/L)^4] \quad \text{at } k = \pm\pi/L . \quad (40)$$

An analytical calculation of the reaction rate $\tilde{\kappa}(L)$ and a numerical calculation of the reactive diffusion coefficient $D^{(r)}(L)$ versus L reveal that

$$\tilde{\kappa}(L) = -\ln \cos \frac{\pi}{L} = \frac{\pi^2}{2L^2} + \mathcal{O}(L^{-4}) , \quad (41)$$

$$D^{(r)}(L) \sim \frac{1}{L} . \quad (42)$$

The reaction rate thus behaves as expected for diffusion-controlled reaction in one dimension, compare to Eq. (10). These results, combined with the results for the diffusive modes, show that, on macroscopic scales, the coarse-grained density and the concentration difference

$$\rho(l) = \int_0^1 dx \int_0^1 dy \tilde{f}(x, y, l) , \quad (43)$$

$$\sigma(l) = \int_0^1 dx \int_0^1 dy g(x, y, l) = G(1, 1, l) , \quad (44)$$

behave like

$$\text{diffusive mode} : \quad \frac{\partial \rho}{\partial t} \simeq D \frac{\partial^2 \rho}{\partial l^2} , \quad (45)$$

$$\text{reactive mode} : \quad \frac{\partial \sigma}{\partial t} \simeq D^{(r)} \frac{\partial^2 \sigma}{\partial l^2} - \tilde{\kappa} \sigma \quad (L \text{ odd}) . \quad (46)$$

Corrections with higher-order spatial derivatives could also be taken into account in the dynamics of the reactive mode. For a model with L odd, this behavior corresponds to a macroscopic diffusion-reaction system with

$$\frac{\partial \rho_A}{\partial t} \simeq \frac{D + D^{(r)}}{2} \frac{\partial^2 \rho_A}{\partial l^2} + \frac{D - D^{(r)}}{2} \frac{\partial^2 \rho_B}{\partial l^2} - \frac{\tilde{\kappa}}{2} (\rho_A - \rho_B) , \quad (47)$$

$$\frac{\partial \rho_B}{\partial t} \simeq \frac{D - D^{(r)}}{2} \frac{\partial^2 \rho_A}{\partial l^2} + \frac{D + D^{(r)}}{2} \frac{\partial^2 \rho_B}{\partial l^2} + \frac{\tilde{\kappa}}{2} (\rho_A - \rho_B) , \quad (48)$$

where $\rho_A = \rho + \sigma/2$ and $\rho_B = \rho - \sigma/2$. According to these macroscopic equations, the diffusion coefficient of each species is $D_A = D_B = (D + D^{(r)})/2$, the cross-diffusion coefficient is $D_{AB} = D_{BA} = (D - D^{(r)})/2$, while the reaction rate of Eq. (2) is given by the logarithm of the absolute value of the leading eigenvalue of the reactive evolution operator as

$$\kappa = \frac{\tilde{\kappa}}{2} = -\frac{1}{2} \ln \cos \frac{\pi}{L} = -\frac{1}{2} \ln |\chi(k=0)| . \quad (49)$$

We remark that, according to the microscopic analysis, the macroscopic equations of a diffusion-reaction system do not necessarily follow the simple assumption often carried out that the cross-diffusion coefficients vanish, $D_{AB} = D_{BA} = 0$. This particular case is only recovered if $D = D^{(r)}$, which is not fulfilled here. The origin of this difference holds in the fact that the diffusion coefficient D_A associated with the state A of a particle is in general different from the diffusion coefficient of the particle itself which may be in two possible states A or B . In this regard, the cross-diffusion appears of importance in reacting systems.

Besides, the models with L even follow more complicated diffusion-reaction equations where the reactive diffusion coefficient $D^{(r)}$ has a different status because it is associated with a nonvanishing wavenumber $k = \pm\pi/L$. Nevertheless, the part of the diffusion-reaction process which is responsible for the reactive exponential decay is confirmed by the microscopic analysis.

B. Reaction rates in the parameter-dependent multibaker

We now discuss the parameter-dependent reactive multibaker by taking the shift parameter h into account, as it has already been done for the purely diffusive case (see Fig. 6). Thus, in addition to the integer periodicity L of the reaction cells of the multibaker the reaction rate κ will also depend on h . One may then raise the question how the reaction rate $\kappa(h, L)$ changes with respect to varying h for fixed L . Moreover, we will give some illustrative features of the time-dependent dynamics of the reaction process for typical h parameters.

Analogously to the previous subsection, we start with the difference of chemical concentrations $g(x, y, l)$ as defined in Eq. (27). We again use the property that parallel to the x -axis the two-dimensional reactive multibaker can be projected onto a one-dimensional map, as has been pointed out before (see Fig. 6). The time evolution of the projected reactive part $\zeta_t(x, l) \equiv \int dy g(x, y, l)$ of the multibaker is then determined by the reactive evolution equation of a respective one-dimensional map,

$$\zeta_t(x, l) = \hat{R}^{(1)}(h, L) \zeta_{t-1}(x, l). \quad (50)$$

Here, $\hat{R}^{(1)}(h, L)$ represents the one-dimensional reactive evolution operator, and $\zeta_t(x, l) \equiv \rho_t(x, l, A) - \rho_t(x, l, B)$ is the difference between A and B -particle densities in the corresponding one-dimensional map. As has been done for the purely diffusive case, we again write this equation as a matrix equation, where instead of $\hat{R}^{(1)}(h, L)$ a topological transition matrix $T(h, L)$ acts onto a particle density vector $\underline{\zeta}_t$. The matrix $T(h, L)$ is structured such that in case of reactive scattering centers the elements in the corresponding columns of the matrix have a negative sign, and thus a particle changes color by leaving a reaction cell. Otherwise, the matrix is the same as discussed for the diffusive case.

We first discuss some details of the time evolution of the reactive modes. By integrating over $\zeta_t(x, l)$ or its respective vector representation we obtain the difference between the total number of A and B -particles at discrete time t which is $\xi_t \equiv \sum_l \int dx \zeta_t(x, l)$. From the corresponding phenomenological time-continuous reaction equation Eq. (46) one would expect that for the reactive multibaker ξ_t decays exponentially after a suitable coarse graining according to $\xi_t = \xi_0 \exp(-\tilde{\kappa}t)$. If this is the case, we can define the reaction rate of the reactive multibaker in analogy to the phenomenological equation as $\kappa(h, L) = \tilde{\kappa}/2$.

To compute $\kappa(h, L)$ according to this definition, we solve the matrix formulation of Eq. (50) by iterating the transition matrices $T(h, L)$ numerically. As an initial particle density we choose $\zeta_0(x, l)$ to be uniform in one reactive cell of the multibaker, which corresponds to having only A particles in this cell with the number of B particles being locally zero, and we make the chain long enough such that the evolving density is not affected by boundary conditions. Fig. 10 (a) and (b) give two typical examples of $\zeta_t(x, l)$ for certain parameter values of h after $t = 40$ iterations. They show how the ‘‘perturbation’’ $\zeta_0(x, l)$, which is a local initial deviation from the equilibrium state $\zeta_t(x, l) = 0$ ($t \rightarrow \infty$), spreads out along the x -axis by exhibiting a rather complex fine structure with oscillations around zero. Fig. 10 (c) and (d) contain half-logarithmic plots of $|\xi_t|$ with respect to the discrete time t . These plots reflect a different dynamical behavior of ξ_t for different magnitudes of the reaction rate. For $\kappa(h, L)$ close to zero, see the upper two curves in Fig. 10 (c), ξ_t decays apparently non-exponentially for small times t . Only for larger times it eventually reaches exponential decay. Thus, the system shows that it is close to states of the h parameter where it is non-reacting. For the lowest curve in Fig. 10 (c), which corresponds to an intermediate reaction rate, ξ_t provides initially strong periodic fluctuations. They are partly due to the complex deterministic dynamics of the reactive baker in one cell of the chain, as has already been observed and explained for a one-dimensional purely diffusive case [32]. Apart from such strong periodic oscillations on a fine scale, in Fig. 10 (d) ξ_t exhibits an interesting crossover between a fast decay for smaller times and a slower decay for larger times, where again it approaches exponential behavior. This may reflect the fact that for larger reaction rates $\kappa(h, L) \gg 0$ the reaction is controlled by the diffusive dynamics. These features of ξ_t should be compared to the characteristics of the respective probability densities $\zeta_t(x, l)$ in the figure.

To obtain quantitative values for the reaction rate, Eq. (50) has been analyzed by solving the eigenvalue problem of the corresponding transition matrix $\mathbf{T}(h, L)$, analogously to what has been done in the previous subsection for the dyadic reactive multibaker. In general, the spectra of $\mathbf{T}(h, L)$ are extremely complicated [48]. However, as has been argued in the previous subsection for special cases, and supported by our observation of long-time exponential decay of ξ_t for the general case, we expect that, in the limit of infinite time, the reaction in the multibaker will always be governed by the slowest eigenmodes and their respective eigenvalues. This motivates to define the parameter-dependent reaction rate $\kappa(h, L)$ via the maximum of the absolute value of the eigenvalues of $\mathbf{T}(h, L)$,

$$\kappa(h, L) \equiv -\frac{1}{2} \ln |\chi_{\max}(h, L)| \quad , \quad (51)$$

analogously to Eq. (49). Numerically, we find that for large regions of the h parameter a certain fundamental domain L_F of the multibaker is sufficient to obtain the correct leading eigenvalue $\chi_{\max}(h, L)$. This domain must always include multiples of two reactive centers, and its length is defined by the number $L_F \equiv 2L \operatorname{Int}(1 + h)$ of cells of the multibaker. In these regions, solutions for the eigenvalue problem of $\mathbf{T}(h, L)$ defined on the domain L_F lead to a maximum eigenvalue $\chi_{\max}(h, L)$ as obtained by solving the corresponding eigenvalue problem for longer and longer chain lengths $mL \rightarrow \infty$, $m \in \mathbb{N}$. However, especially for small L and large $\kappa(h, L)$ this fundamental domain only provides an approximation to the exact results which are then obtained by making the chain length mL large enough such that the error in $\chi_{\max}(h, L)$ with respect to mL is sufficiently small. Fig. 11 shows some typical largest eigenmodes $\psi(x, l)$ on the fundamental domain in cases where it gives the correct corresponding largest eigenvalue $\kappa(h, L)$. For large reaction rates, to a certain respect the largest eigenmodes behave like sine functions, see Fig. 11 (a), whereas for smaller reaction rates, the largest eigenmodes approach two-periodic step-like functions as shown in Fig. 11 (b). Fig. 11 (c) depicts the largest eigenmodes for a parameter value of h which is just at the borderline of a non-reacting h region, but where the system is nevertheless already highly reactive. Here, the eigenmodes appear to be especially complicated [48].

In Fig. 12 (a) the reaction rate $\kappa(h, L)$ as defined via Eq. (51) has been computed for a series of reaction center periodicities L . For $h = 0.25$ there is no reaction rate in the system. In this case, the iteration method confirms that the difference in the number of particles ξ_t oscillates periodically around zero instead of decaying exponentially. An analysis of the eigenvalue spectra of the corresponding transition matrices reveals that at this h parameter the respective reactive multibakers are not ergodic [48]. For all other h of the figure the reaction rate is well-defined and shows a complicated structure. By increasing L the reaction rate $\kappa(h, L)$ decreases almost everywhere, as one can expect intuitively, except in certain small parameter regions of h . Fig. 12 (b) gives the full result for $\kappa(h, L)$ at $L = 2$. This structure repeats itself with a periodicity of $2m \leq h \leq 2 + 2m$, $m \in \mathbb{N}_0$. In certain intervals of h the four peaks depicted in the figure are very similar, or even identical, however, there does not appear to be a simple scaling law by which the full peaks can be mapped onto each other. The plateau regions with zero reaction rate correspond to the respective regions observed in Fig. 7 for the diffusion coefficient of the system. They share the same characteristics as discussed above for the singular case of $h = 0.25$, except that at $h = 1$ the system is ergodic, but not mixing. Topologically, these regions are of the same origin as explained for the diffusive case. In Fig. 7 (c) the reaction rate has been computed for $L = 3$. In contrast to the two-periodic case the change from a non-reactive region to a reactive region occurs for $L = 3$ apparently discontinuously in the reaction rate by varying h around 1. This corresponds to the system at $h = 1$ and $L = 3$ being mixing, whereas for the same h and $L = 2$ it was ergodic, but not mixing. We note that for $L = 4$ there are even two of such discontinuous transitions. The detailed irregular structure of the curves, as well as the phase-transition like behavior shown in Fig. 12 (c), can be understood in more detail by analyzing the eigenvalue spectra of the reactive evolution operator and how they change under parameter variation, as will be discussed elsewhere [48].

Apart from varying h , other parameter dependencies can be studied in this reactive multibaker as well. For example, the distance between the single reaction centers could be changed by allowing L to be continuous, the positions of the reaction centers could be shifted by keeping L fixed, and the size of the reaction centers could be increased or decreased. In all these cases we expect non-trivial parameter dependences to be typical which are similar to the one depicted in Fig. 12 [48].

V. DISCUSSION AND CONCLUSIONS

In this paper, we have analyzed simple deterministic models of diffusion-controlled reaction. The models fulfill the chaotic hypothesis mentioned in the Introduction, which allows us a much sharper analysis of the phenomenological foundation of diffusion-reaction processes than with the old stochastic assumption. In this regard, for the simplest model we have been able to derive the exact dispersion relations not only of the diffusive modes but also of the reactive

modes. The reactive modes indeed decay exponentially, as it should be for nonconserved quantities. The reaction rate behaves like $\kappa \sim D/L^2$, as expected for diffusion-controlled reactions in one dimension. The reaction rate introduces a new time scale $T_{\text{react}} \sim \kappa^{-1} \sim L^2/D$, with respect to purely diffusive systems. This reactive time depends on the concentration $\sim 1/L$ of catalysts and, therefore, it takes a fixed value in a given diffusion-reaction system. This time scale of reaction is intermediate between the short time scale of the Lyapunov instability $T_{\text{chaos}} \sim \lambda_{\text{max}}^{-1}$ and the long time scale of diffusion $T_{\text{diff}} \sim L^2/D$. An important difference between diffusion and reaction is that the evolution operator is positive in the diffusive subspace and is thus of Frobenius-Perron type, although the evolution operator (28) has both signs in the reactive subspace. By analyzing this deterministic evolution operator, we have found that the spatial dynamics of the reactive modes appears significantly different from the standard assumption of macroscopic diffusion-reaction models due to the particular importance of cross diffusion. On the other hand, the eigenstates associated with the reactive and diffusive modes are expressed as singular Schwartz distributions, also in contrast with the phenomenological models which have always suggested that the eigenstates are regular functions. In a sense, we may say that this singular character of the exact eigenmodes renders their relaxation compatible with the deterministic dynamics of the particles, in full respect to the mechanical Liouville theorem of volume preservation. This result previously observed for diffusion is here shown to hold also for reaction.

Moreover, the macroscopic transport coefficients such as the diffusion coefficient and the reaction rate both turn out to exhibit a highly irregular behavior as a function of a control parameter of the system. In this way, we have pursued the early work by Elskens and Kapral who studied the isomerization rate for the simplest values of their model parameter [19]. The irregular behavior has its origin in the topological instability of the trajectories in phase space and also in the singular character as represented by Takagi functions. It appears as a fundamental result because the topological instability of phase-space dynamics is a common feature to many systems including the Lorentz gas, the hard-sphere gas, and nonhyperbolic systems which are all non-robust under parametric perturbations. However, we may expect that the transport coefficients would have an irregular behavior only if the systems fulfill certain additional criteria, as being spatially periodic, being sufficiently low-dimensional, and being such that particle-particle interactions are not of main importance. Physical systems of this kind could - to a certain extent - already be realized experimentally in form of so-called antidot lattices [46]. On the other hand, the detailed fractal character of parameter-dependent transport coefficients may disappear by increasing the number of degrees of freedom, or by including strong stochastic perturbations [47]. We have moreover observed that the reaction rate is not only a highly irregular function of the parameter but also presents discontinuities which are reminiscent of nonequilibrium phase transitions. The parametric sensitivity seems thus enhanced at the level of the reactive properties as compared with the diffusive ones.

Acknowledgements. The authors want to thank Prof. G. Nicolis for continuous support and encouragement. They also want to thank Prof. T. Tél for inviting them to the summer school/workshop “Chaos and Irreversibility” (Eötvös University, Budapest, August/September 1997) and for his hospitality. P.G. is financially supported by the National Fund for Scientific Research (F. N. R. S. Belgium). This research is partly financially supported by the IUAP-PAI Program of the Belgian Federal Office SSTC and by the “Human Capital and Mobility Program” of the European Commission. R.K. gratefully acknowledges a grant from the Deutsche Forschungsgemeinschaft (DFG).

-
- [1] J. R. Dorfman, *From molecular chaos to dynamical chaos*, Lecture Notes (University of Maryland, College Park, 1996).
 - [2] D. J. Evans, G. P. Morriss, *Statistical Mechanics of Nonequilibrium Liquids* (Academic Press, London, 1990); W. G. Hoover, *Computational Statistical Mechanics* (Elsevier, Amsterdam, 1991).
 - [3] P. Gaspard, *Chaos, Scattering, and Statistical Mechanics* (Cambridge University Press, Cambridge, 1998).
 - [4] D. J. Evans, E. G. D. Cohen, and M. P. Morris, Phys. Rev. A **42**, 5990 (1990); N. I. Chernov, G. L. Eyink, J. L. Lebowitz, and Ya. G. Sinai, Phys. Rev. Lett. **70**, 2209 (1993).
 - [5] P. Gaspard and G. Nicolis, Phys. Rev. Lett. **65**, 1693 (1990).
 - [6] R. Klages and J.R. Dorfman, Phys. Rev. Lett. **74**, 387 (1995).
 - [7] W. Breymann, T. Tél, and J. Vollmer, Phys. Rev. Lett. **77**, 2945 (1996).
 - [8] R. Livi, A. Politi, and S. Ruffo, J. Phys. A: Math. Gen. **19**, 2033 (1986).
 - [9] H. A. Posch and W. G. Hoover, Phys. Rev. A **38**, 473 (1988); **39**, 2175 (1989); Ch. Dellago and H. A. Posch, Phys. Rev. E **52**, 2401 (1995); Ch. Dellago, H. A. Posch, and W. G. Hoover, Phys. Rev. E **53**, 1485 (1996).
 - [10] H. van Beijeren and J. R. Dorfman, Phys. Rev. Lett. **74**, 4412 (1995); M. H. Ernst et al., Phys. Rev. Lett. **74**, 4416 (1995); A. Latz, H. van Beijeren, and J. R. Dorfman, Phys. Rev. Lett. **78**, 207 (1997).
 - [11] N. S. Krylov, *Works on the Foundations of Statistical Physics* (Princeton University Press, Princeton, 1979).
 - [12] P. Gaspard, in: *Solitons and Chaos*, I. Antoniou and F. Lambert, Eds. (Springer, Berlin, 1991) pp. 46-57.
 - [13] P. Gaspard and F. Baras, Phys. Rev. E **51**, 5332 (1995).

- [14] J. R. Dorfman and P. Gaspard, Phys. Rev. E **51**, 28 (1995).
- [15] P. Gaspard and J. R. Dorfman, Phys. Rev. E **52**, 3525 (1995).
- [16] G. Gallavotti and E. G. D. Cohen, Phys. Rev. Lett. **74**, 2694 (1995); J. Stat. Phys. **80**, 931 (1995).
- [17] P. Gaspard, Adv. Chem. Phys. **99**, 369 (1997).
- [18] P. Glansdorff and I. Prigogine, *Thermodynamics of Structure, Stability, and Fluctuations* (Wiley, New York, 1971); G. Nicolis and I. Prigogine, *Self-Organization in Nonequilibrium Systems* (Wiley, New York, 1977); G. Nicolis and M. Malek Mansour, Prog. Theor. Phys. Suppl. **64**, 249 (1978); G. Nicolis, *Introduction to Nonlinear Science* (Cambridge University Press, Cambridge, 1995); F. Baras and M. Malek Mansour, Adv. Chem. Phys. **100**, 393 (1997).
- [19] Y. Elskens and R. Kapral, J. Stat. Phys. **38**, 1027 (1985).
- [20] L. A. Bunimovich and Ya. G. Sinai, Commun. Math. Phys. **78**, 247, 479 (1980).
- [21] N. I. Chernov, J. Stat. Phys. **74**, 11 (1994).
- [22] P. Gaspard, Phys. Rev. E **53**, 4379 (1996).
- [23] P. Gaspard, J. Stat. Phys. **68**, 673 (1992).
- [24] P. Gaspard, Chaos **3**, 427 (1993).
- [25] P. Gaspard, in: *Dynamical Systems and Chaos*, Y. Aizawa, S. Saito, and K. Shiraiwa, Eds. (World Scientific, Singapore, 1995) vol. 2, pp. 55-68.
- [26] S. Tasaki and P. Gaspard. In M. Yamaguti, editor, *Towards the Harnessing of Chaos*, pages 273–288 (Elsevier, Amsterdam, 1994); S. Tasaki and P. Gaspard, J. Stat. Phys. **81**, 935–987 (1995).
- [27] G. H. Weiss, J. Stat. Phys. **42**, 3 (1986); B. J. Berne, M. Borkovec, and J. E. Straub, J. Phys. Chem. **92**, 3711 (1988).
- [28] M. Hata and M. Yamaguti, Jpn. J. Appl. Math. **1**, 183 (1984).
- [29] J. L. Lebowitz, Phys. Rev. **114**, 1192 (1959); J. A. MacLennan Jr., Phys. Rev. **115**, 1405 (1959); P. Gaspard, Physica A **240**, 54 (1997).
- [30] P. Gaspard, J. Stat. Phys. **88**, 1215 (1997).
- [31] M. Schell, S. Fraser, and R. Kapral, Phys. Rev. A, **26**, 504 (1982); H. Fujisaka and S. Grossmann, Z. Physik B **48**, 261 (1982); T. Geisel and J. Nierwetberg, Phys. Rev. Lett. **48**, 7 (1982).
- [32] R. Klages, *Deterministic diffusion in one-dimensional chaotic dynamical systems* (Wissenschaft und Technik-Verlag, Berlin, 1996).
- [33] R. Klages and J.R. Dorfman, Phys. Rev. E **55**, R1247 (1997).
- [34] R. Klages and T. Tél, *Deterministic transport in time-reversible area-preserving and dissipative dynamical systems*, preprint (1997).
- [35] R. Klages, J. R. Dorfman, and P. Gaspard, *Fractal forms in a Green-Kubo formula for simple deterministic dynamical systems*, preprint (1995).
- [36] Chr. Beck and F. Schlögl, *Thermodynamics of Chaotic Systems* (Cambridge University Press, Cambridge, 1993); A. Boyarsky, J. Stat. Phys. **50**, 213 (1988).
- [37] Solving the Frobenius-Perron equation this way for the *full* chain of maps instead of only for one box provides two further methods to compute diffusion coefficients, without employing the Green-Kubo formula [32]. Moreover, it is possible to refine the transition matrix approach such that explicitly one does not have to deal with Markov partitions anymore [42].
- [38] J. Groeneveld, priv. commun.
- [39] M. Doerfle, J. Stat. Phys. **40**, 93 (1985); S. V. Ershov, Phys. Lett. A **177**, 180 (1993); R. Kluiving, H. W. Capel, R. A. Pasmanter, Physica A **164**, 593 (1990).
- [40] J.A.G. Roberts, G. R. W. Quispel, Phys. Rep. **216**, 63 (1992); R. Klages, *Phase space densities and Lyapunov exponents in time-reversible discrete dynamical systems*, preprint (1997).
- [41] If h takes integer values, we find for \mathbf{G} a simple mirroring along the diagonal $x = y$ in each unit cell. If h takes odd multiples of $1/2$, by shifting all unit cells about $\Delta x = 1/2$ we find for \mathbf{G} a mirroring along the diagonal from the upper left to the lower right in each unit cell.
- [42] R. Klages, *Simple deterministic dynamical systems with drift: negative currents and suppression of diffusion*, preprint (1997).
- [43] T. Tél, J. Vollmer, and W. Breyman, Europhys. Lett. **35**, 659 (1996); J. Vollmer, T. Tél, and W. Breyman, Phys. Rev. Lett. **79**, 2759 (1997).
- [44] B. Moran, W. G. Hoover, Journ. Stat. Phys. **48**, 709 (1987); J. Lloyd et al., Chaos **5**, 536 (1995); Ch. Dellago, L. Glatz, H. A. Posch, Phys. Rev. E **52**, 4817 (1995); Ch. Dellago, priv. commun.; C. Dettmann, priv. commun.; C. Dettmann, G.P. Morriss, Phys. Rev. Lett. **78**, 4201 (1997).
- [45] P. Jung, J. G. Kissner, and P. Haenggi, Phys. Rev. Lett. **76**, 3436 (1996); P. Haenggi and R. Bartussek, *Brownian rectifiers: How to convert Brownian motion into directed transport*. in: J. Parisi et al. (Eds), *Nonlinear Physics of Complex Systems*. Springer Series 'Lecture Notes in Physics' (Springer, Berlin, 1996); and further references therein.
- [46] see, e.g., D. Weiss et al., Phys. Rev. Lett. **66**, 2790 (1991), and further references therein.
- [47] G. Radons, Phys. Rev. Lett. **77**, 4748 (1996); R. Klages, *Enhancement and suppression of deterministic diffusion by random perturbations*, preprint (1996).
- [48] P. Gaspard, R. Klages, unpublished.

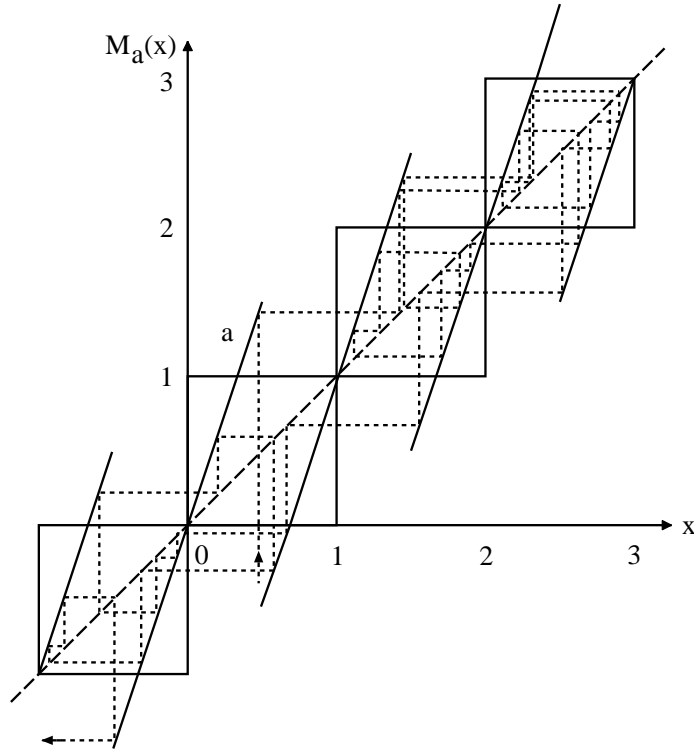


FIG. 3. A simple model for deterministic diffusion. The slope a , here $a = 3$, serves as a control parameter in the periodically continued piecewise linear map.

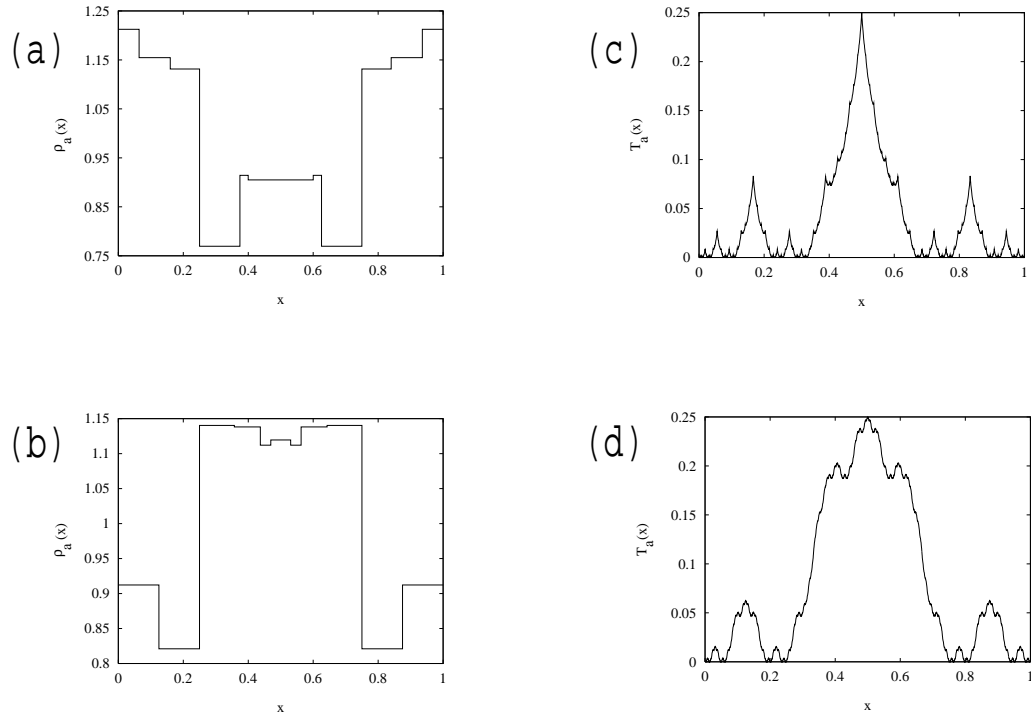


FIG. 4. (a), (b) Invariant probability densities $\rho_a(x)$ on the unit interval for the map of Fig. 3 modulo 1. The slope is $a \simeq 2.5004$ for (a) and $a \simeq 3.49997$ for (b). (c), (d) Generalized Takagi functions $T_a(x)$ for the same map at $a = 3$ in (c) and at $a = 4$ in (d).

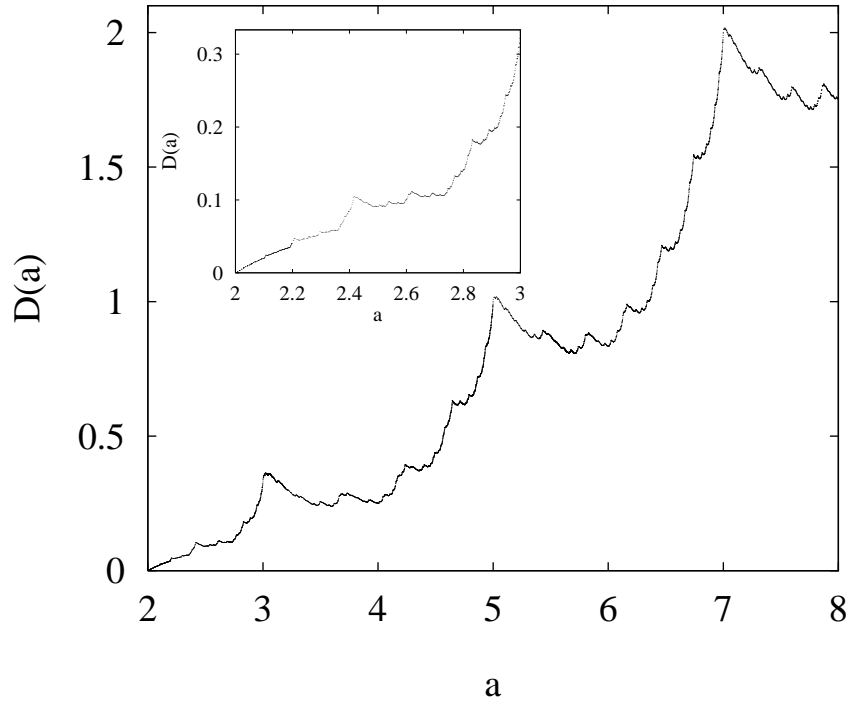


FIG. 5. Parameter-dependent diffusion coefficient $D(a)$ for the map of Fig. 3 and blowup of the initial region. The main graph consists of 7,908 single data points, the magnification of 979. In both cases errorbars are too small to be visible.

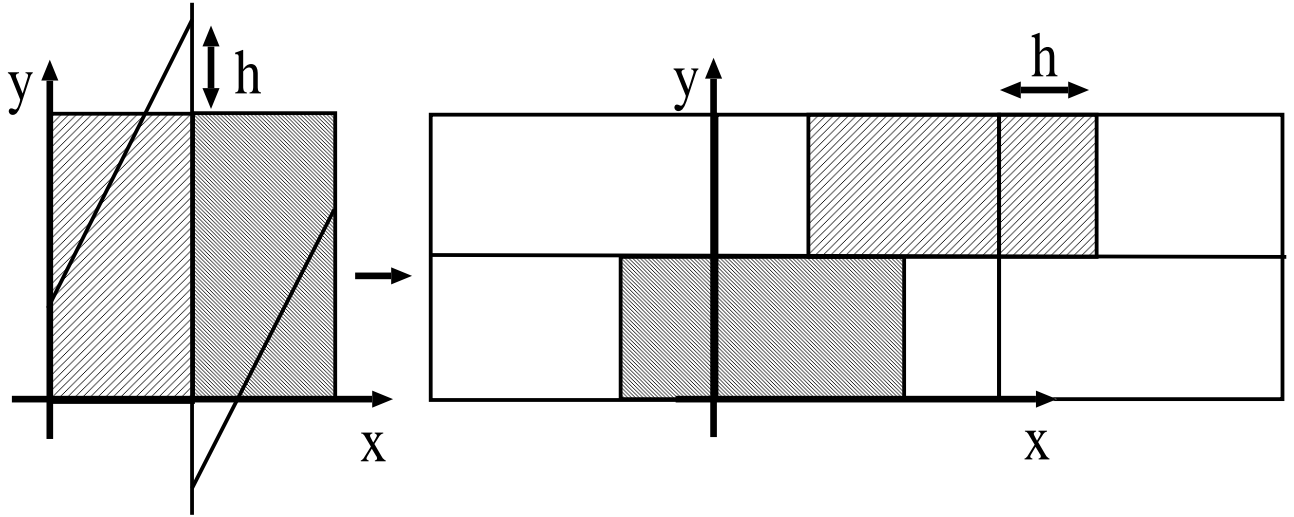


FIG. 6. Dynamics of one cell of an area-preserving time-reversible multibaker with a non-trivial parameter-dependence h . Projection of the dynamics onto the horizontal axis reduces the system to the symmetric one-dimensional piecewise linear map shown in the figure to the left which for $h = 0$ is the Bernoulli shift.

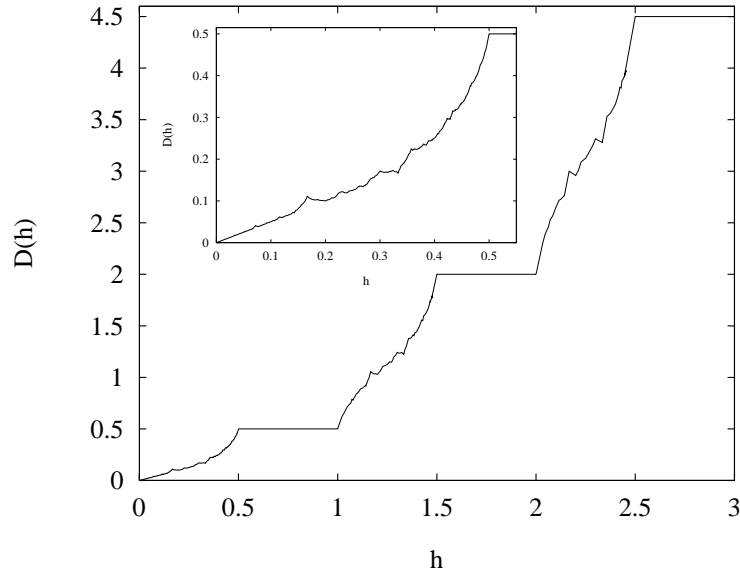


FIG. 7. Parameter-dependent diffusion coefficient $D(h)$ for the multibaker of Fig. 6 and blowup of the initial region. The main graph consists of 638 data points, the magnification of 514. In both cases the single points have been connected with lines, errorbars are too small to be visible.

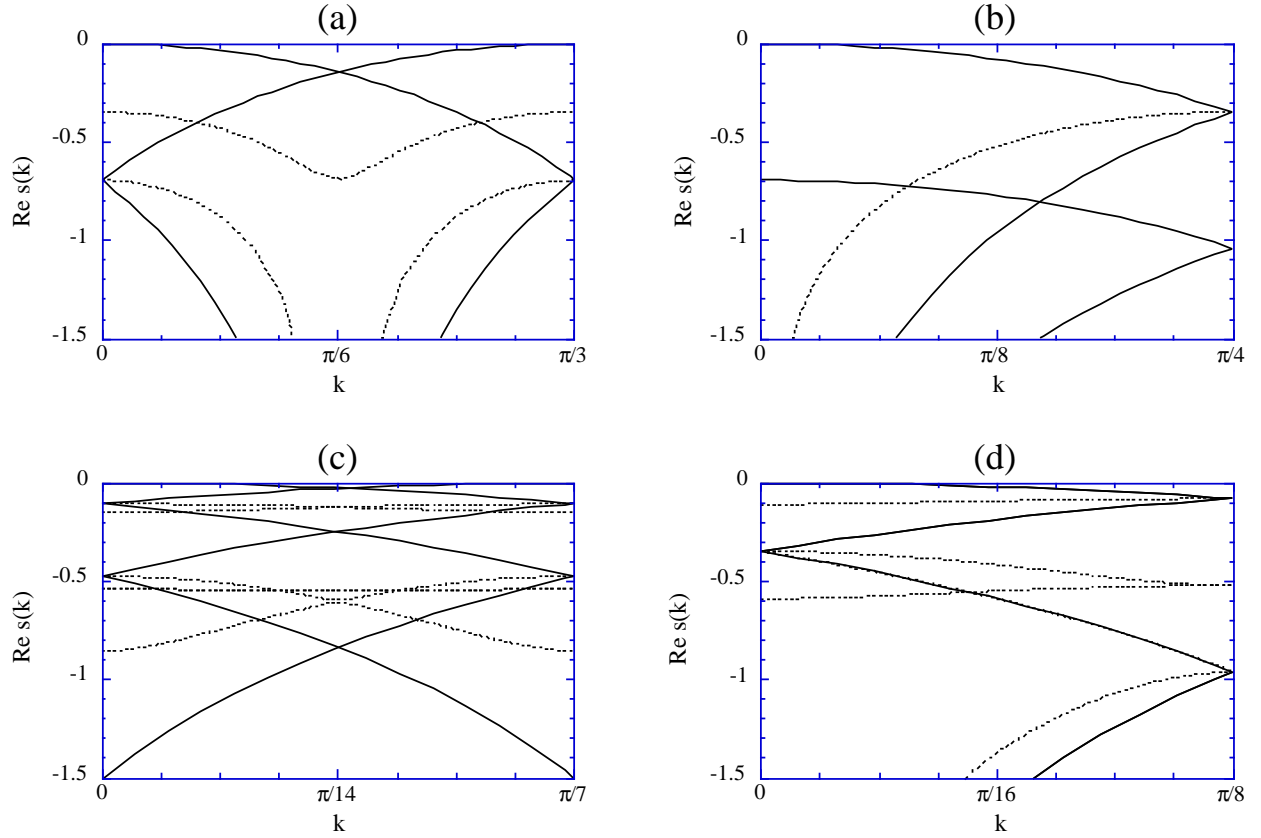


FIG. 8. Dispersion relations of the diffusive modes (solid lines) and of the reactive modes (dotted lines) for the dyadic reactive multibaker with (a) $L = 3$; (b) $L = 4$; (c) $L = 7$; (d) $L = 8$. (note: poor quality output; the originals can be obtained upon request)

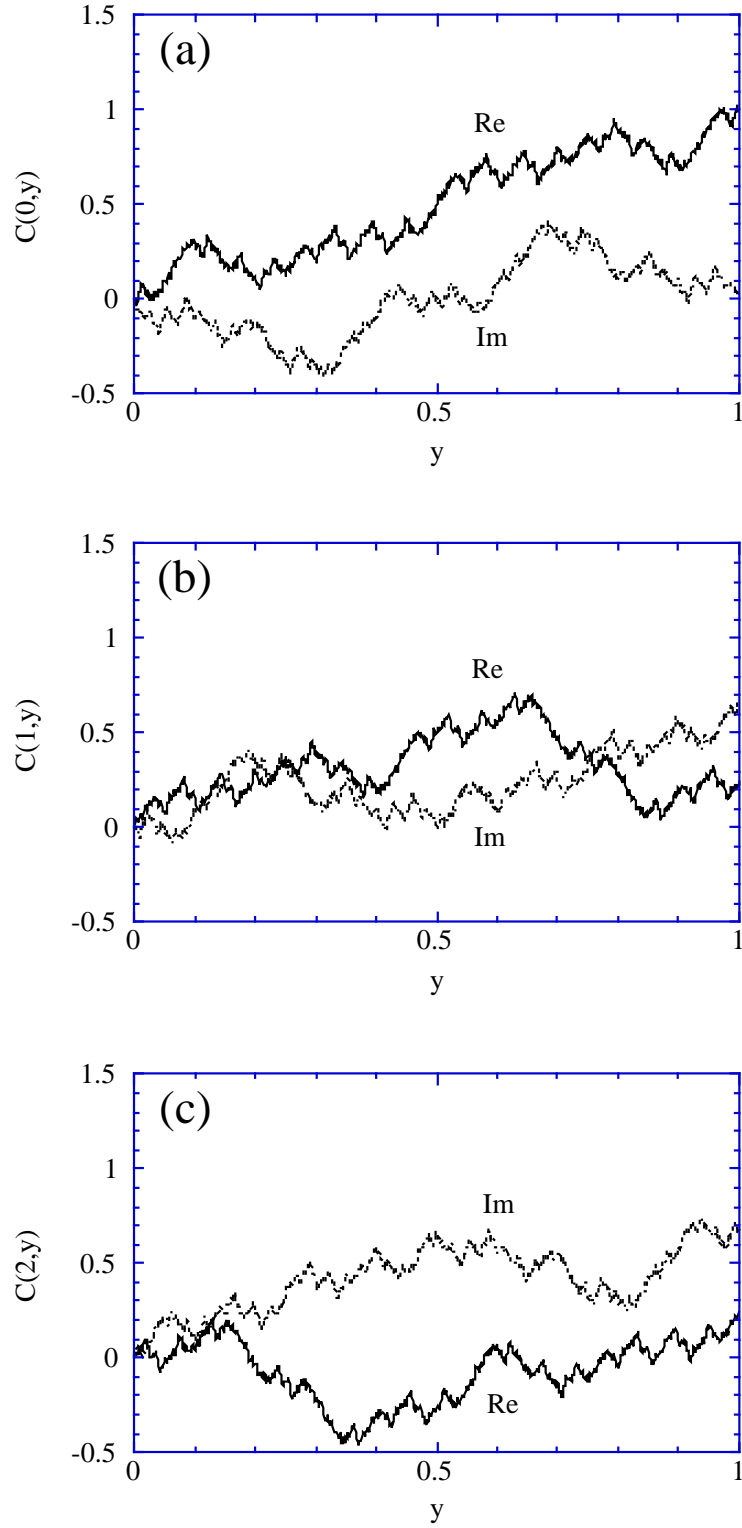


FIG. 9. Cumulative functions $\{C(y, l)\}$ with $l = 0, 1, 2$ of the reactive eigenstate at vanishing wavenumber $k = 0$ in the reactive multibaker model $L = 3$. (note: poor quality output; the originals can be obtained upon request)

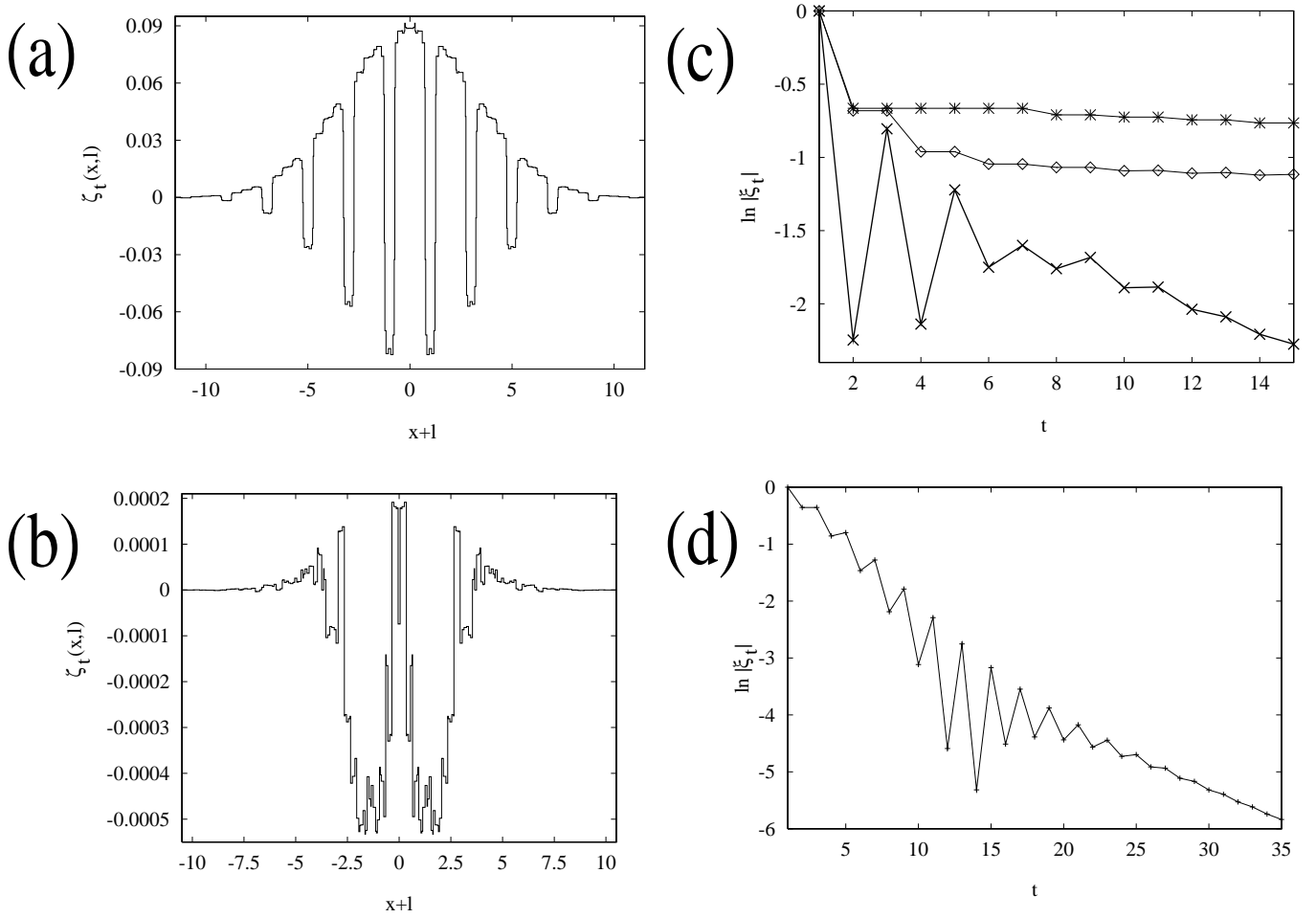


FIG. 10. (a), (b) Densities corresponding to the difference in the number of A and B -particles per total number of particles after $t = 40$ iterations of the map. In (a) ($L = 2, h \simeq 0.2429$) the reaction rate is close to zero, whereas in (b) ($L = 3, h \simeq 0.1496$) it is locally maximal in h . (c), (d) Half-logarithmic plots of the total difference ξ_t in the number of A and B -particles of the system as it varies in time t . In (c) the corresponding reaction rates $\kappa(h, L)$ are close to zero for the upper two curves ($\kappa < 0.006$), for the lower curve the reaction rate has an intermediate value ($\kappa \simeq 0.02$), whereas in (d) it is locally maximal in h ($\kappa \simeq 0.05$). The parameters for the upper curve in (c) correspond to (a), the curve in the middle is at $L = 3, h \simeq 0.247$, and the lowest one is at $L = 3, h \simeq 0.4472$. Case (d) corresponds to (b).

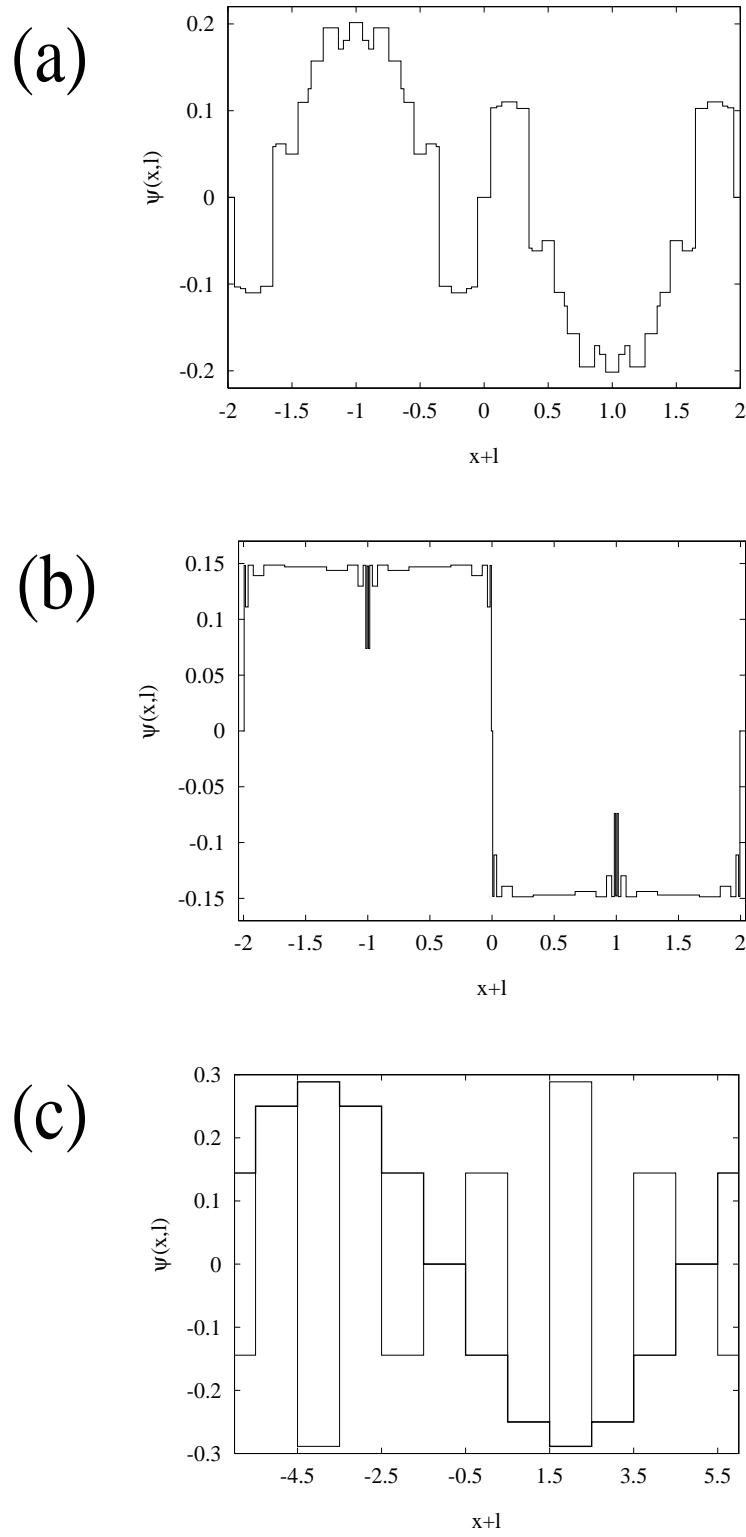


FIG. 11. Examples of largest eigenmodes $\psi(x, l)$ for the reactive multibaker corresponding to the largest eigenvalue $\chi_{\max}(h, L)$ parallel to the x axis in the fundamental domain L_F as described in the text. For (a) ($L = 2, h \simeq 0.1496$) the reaction rate $\kappa(h, L)$ is very large ($\kappa \simeq 0.12$), for (b) ($L = 2, h \simeq 0.4947$) it is very small ($\kappa \simeq 0.003$). In both cases, there exist only two real largest eigenmodes where the second ones are shifted by a phase. In (c) ($L = 6, h = 1$) both largest eigenmodes have been plotted (thick line for the one and thin line for the other, respectively).

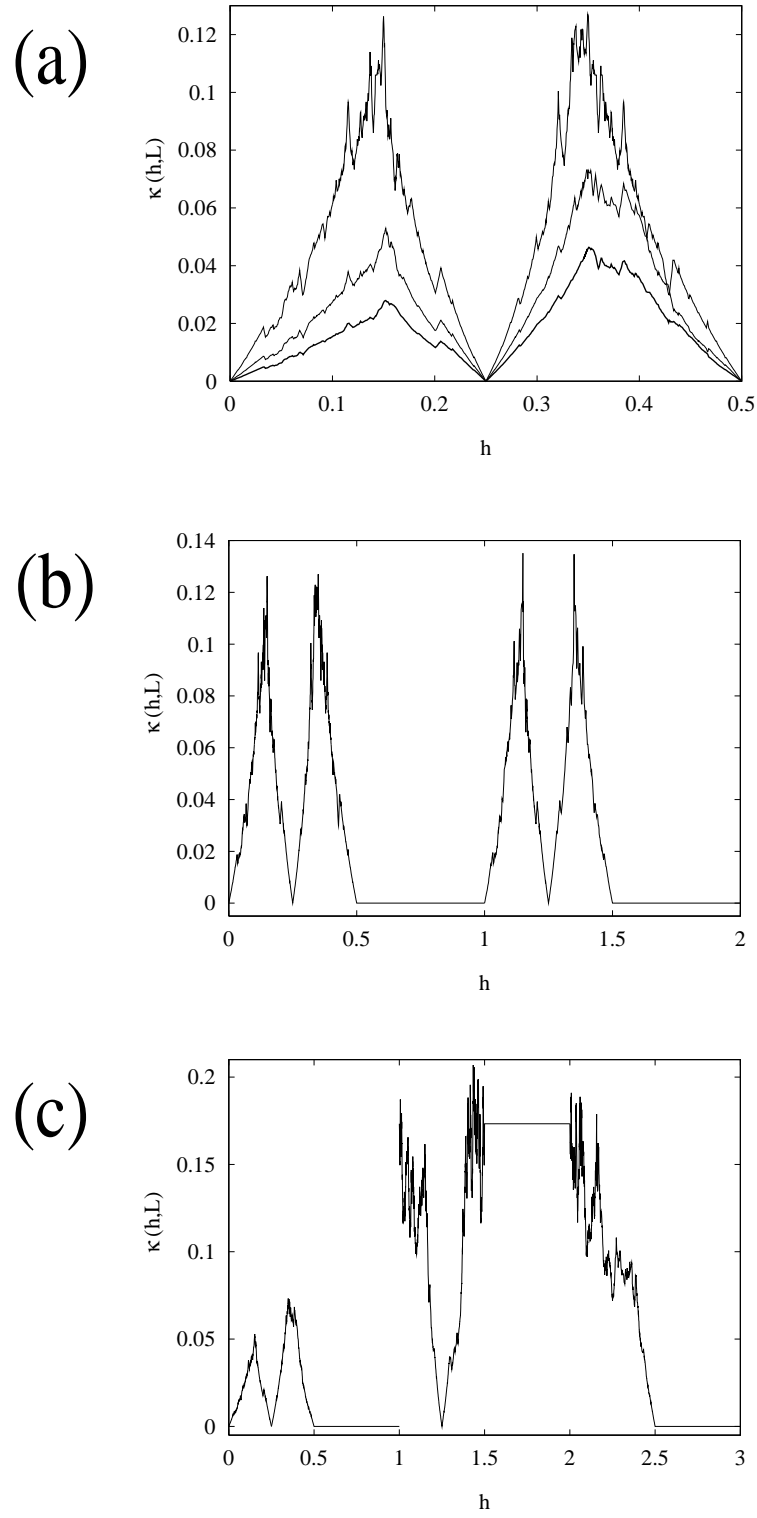


FIG. 12. (a) Reaction rate $\kappa(h, L)$ at different integer values of the reaction cell periodicity: $L = 2$ (upper curve), $L = 3$ (middle), $L = 4$ (lower curve). (b) Reaction rate for $0 \leq h \leq 2$ at $L = 2$. (c) Reaction rate for $0 \leq h \leq 3$ at $L = 3$. In all cases, error bars are too small to be visible.